Experimental Flow Studies in PDMS Intracranial Aneurysms Manufactured by Two Different Techniques

Andrews Souza[1,2,3] [a], Inês Afonso[1,3] [b], Violeta Carvalho[1,2,4,5] [c], Diana F. Rodrigues[1],
Senhorinha Teixeira[4] [d], João Eduardo Ribeiro[3] [e], José Eduardo Socha Pereira[6] [f],
Reinaldo Rodrigues de Souza[1,6] [g], Rui Lima[1,7] [h] and Ana Sofia Moita[6] [i]

[1]MEtRICs, Mechanical Engineering Department, University of Minho, Campus de Azurém, 4800-058 Guimarães, Portugal
[2]Center for MicroElectromechanical Systems (CMEMS-UMinho), University of Minho,
Campus de Azurém, 4800-058 Guimarães, Portugal
[3]Campus de Santa Apolónia, CIMO—Instituto Politécncio de Bragança, 5300-253 Bragança, Portugal
[4]ALGORITMI/LASI Center, University of Minho, Campus de Azurém, 4800-058 Guimarães, Portugal
[5]LABBELS—Associate Laboratory, Braga/Guimarães, Portugal
[6]IN+, Center for Innovation, Technology and Policy Research, Instituto Superior Técnico, Universidade de Lisboa,
Av. Rovisco Pais, 1049-001, Lisboa, Portugal
[7]CEFT, Faculdade de Engenharia da Universidade do Porto (FEUP), Rua Roberto Frias, 4200-465, Porto, Portugal
[8]ALiCE - Associate Laboratory in Chemical Engineering, Faculty of Engineering, University of Porto,
Rua Dr. Roberto Frias, 4200-465 Porto, Portugal

Keywords: Intracranial Aneurism Biomodels, PDMS, In vitro Flow Test, Biofluids, Additive Manufacturing, Polysmooth.

Abstract: The aim of this study was to investigate the flow within intracranial aneurysms, which are localized dilations of the cerebral arteries that pose a risk of rupture and strokes. The experimental analysis was conducted on scaled-down biomodels of a cerebral aneurysm to better understand its flow patterns. To carry out the experimental phase, the biomodels were manufactured using rapid prototyping and lost core casting techniques. The biomodels were assessed for optical transparency and dimensions, confirming their suitability for flow visualization tests. The findings revealed that within the recirculation zones of the aneurysm, the flow velocities were notably lower when compared to the entry and exit points. As the flow rate increased, the recirculation focus gradually approached the aneurysm wall. Furthermore, the geometry of the aneurysm played an important role in influencing the flow behavior. These insights are crucial, as they are linked to some extent with the risk of intracranial aneurysm rupture, which may entail severe consequences. This study enriches our understanding of the aneurysm flow dynamics and contributes to the development of the inherent preventative and treatment measures.

1 INTRODUCTION

Intracranial aneurysms are localized dilations of the arteries in the brain (Rodriguez-Régent *et al.,* 2014).

These dilations can weaken the blood vessel wall and increase the risk of rupture, becoming a significant cause of cerebrovascular accidents. They usually develop in the major arteries of the cerebral

[a] https://orcid.org/0000-0003-2414-073X
[b] https://orcid.org/0000-0001-6416-2867
[c] https://orcid.org/0000-0002-9447-4746
[d] https://orcid.org/0000-0002-7464-3944
[e] https://orcid.org/0000-0001-6300-148X
[f] https://orcid.org/0000-0001-7244-8611
[g] https://orcid.org/0000-0001-5250-820X
[h] https://orcid.org/0000-0003-3428-637X
[i] https://orcid.org/0000-0001-9801-7617

circulation, particularly in specific locations within the so-called "Willis polygon" (Lasheras, 2007). Some studies have identified that the anterior cerebral artery is involved in around 40% of cases of intracranial aneurysm rupture (Inagawa 2010; Ye *et al.* 2017).

These aneurysms can be classified into two main groups based on their geometry and location: fusiform and saccular, with saccular aneurysms being the most common type, representing approximately 90% of cases (Lasheras 2007). Blood flow within aneurysms depends on various factors, including the size, shape of the aneurysm, and the geometry of the originating artery (Ye *et al.* 2017).

To study these aneurysms, there are experimental and numerical approaches. Experimental approaches typically involve creating in vitro models that simulate blood flow and artery deformation. Studies show that the initial models were made of glass (Ferguson, 1972), and later, silicone models emerged (Steiger *et al.* 1988). Currently, they have been produced using PDMS (Souza *et al.*, 2020). In this regard, various techniques have been applied to these models, such as Magnetic Resonance, Doppler Laser, Digital Image Correlation, PTV (Particle Tracking Velocimetry), and PIV (Particle Image Velocimetry) (Steiger *et al.* 1988; Roloff *et al.* 2013; Souza, 2020b). It should be noted that the most used experimental technique to validate numerical simulations is the PIV technique.

Manufacturing technology has evolved, using materials like PDMS (polydimethylsiloxane) to create aneurysm models. PDMS is chosen due to its hyper elasticity, biocompatibility, and cost-effectiveness (Miranda, 2022).

The manufacturing and subsequent experimental studies of representative biomodels of a cerebral aneurysm, with mechanical properties close to those of arteries, are of utmost importance to understand the phenomena responsible for the growth and rupture of intracranial aneurysms (Souza *et al.*, 2020; Rodrigues *et al.* 2016). Therefore, the current work has the primary objective of studying the blood flow in a representative biomodel of a cerebral aneurysm, specifically focusing on the fabrication of semi-rigid optimized biomodels suitable for experimental flow visualization.

In this regard, and considering the manufacturing processes studied, IA (Intracranial Aneurism) biomodels were manufactured. The first biomodel was made using a manufacturing process described in more detailed at Souza *et al.,* 2020. Briefly, the manufacture of the aneurysm lumen involves a combination of additive manufacturing methods and

a lost core casting process using glycerin-based soap. The second one was manufactured using the FDM (Fused Deposition Modelling) technique and the material used was polysmooth. This material allows surface treatment with isopropyl alcohol to smooth out the roughness from the printing process. At the end of both processes, the lumens obtained are positioned in an acrylic box where the PDMS were casted by gravity and cured for 48 hours at room temperature. The results of this work have shown that the biomodels of beeswax and glycerine-based soap were the most suitable in vitro models to perform direct flow visualizations of particulate blood analogue fluids. The authors proposed an effective manufacturing method from real flow biomodels, at the millimeter scale and suitable for hemodynamic studies.

2 MATERIALS AND METHODS

2.1 Experimental Setup

For the experimental flow visualization tests, a set interconnected equipment was essential. Two key components worth mentioning include the high-speed video device, which primarily featured a Photron FASTCAM high-speed camera, complemented by visualization software for post-processing and analysis. In addition, an inverted microscope model *IX71* from Olympus™ was also used, together with a *N-Achroplan* 2.5x/0.07 objective. Figure 1 illustrates the primary equipment employed in this study, including the high-speed camera, inverted microscope, syringe pump, PDMS biomodel, and acquisition system.
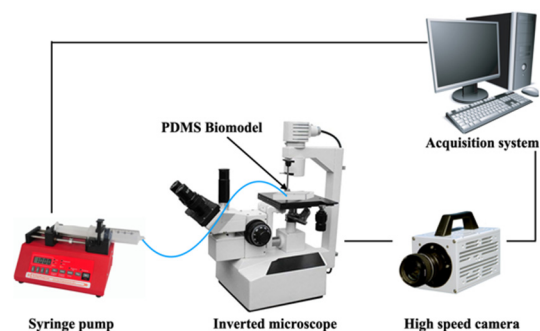

Figure 1: Schematic representation of the experimental setup.

2.2 Evaluation of the Optical Transparency of the Biomodel

When studying biomodels, certain limitations must be considered. One of these restrictions pertains to optical properties, specifically the requirement that the material used for the external biomodel must be transparent, and its refractive index should closely match that of the fluid used in experiments. This alignment of refractive indexes is crucial to facilitate experimental flow visualization tests on the PDMS biomodels.

In cases where there is a significant disparity between the refractive index of the fluid and that of the PDMS, distortions may appear near the walls. However, this distortion can be mitigated or eliminated when the refractive index of the fluid closely matches that of the biomodel material (Souza *et al.*, 2020).

It is important to bear this update issue in mind, as it may subsequently have a negative influence on the visualization of particles when carrying out the experimental tests.

Thus, in the present study, with the aim of evaluating the optical transparency of the biomodel, two fluids with different physical properties were considered, so that it was possible to make a comparison and perceive the differences between them. Therefore, one of the used fluids, which has a refractive index very similar to that of PDMS, was a mixture of liquid glycerin and distilled water, that is, 61 grams of liquid glycerin were diluted in distilled water (61% w/w). The second used fluid was only water.

It is important to mention that the application of this technique, to evaluate the optical transparency of the biomodel under study, was based on the work of Hopkins *et al.,* 2000.

The physical properties of the materials used in the present study are summarized in Table 1: Physical properties of the employed materials to evaluate the optical transparency of biomodels.. It should be noted that these properties were considered as explained in (Souza *et al., 2020*).

Table 1: Physical properties of the employed materials to evaluate the optical transparency of biomodels.

Material	Refractive Index	Viscosity (Pa. s)	Density (kg/m^3)
Water	1.333	9.20×10^{-4}	997
Glycerin mixture	1.412	1.29×10^{-2}	1153
PDMS	1.412	-	

2.3 Flow Visualization Experimental Testing

In the initial step, the PDMS biomodel was secured under the microscope. Subsequently, a syringe pump system, utilizing a *Terumo™* 50 mL syringe, was employed to deliver the working fluid at a fixed flow rate. This fluid was pumped not only through the channels connecting the syringe to the biomodel but also within the biomodel itself.

The fluid used in this flow visualization experiment was a mixture of liquid glycerin and 61% distilled water (w/w). Additionally, 0.06% PMMA (polymethylmethacrylate) particles with a 60 μm diameter were suspended in this fluid. It's worth noting that the selection of this fluid was based on previous work conducted by Campo-Deaño *et al.* (2013) and Pinho *et al.* (2017). Table 1 presents the physical properties of the fluid under investigation, including density, refractive index, and viscosity with the suspended particles.

The primary objectives of this experimental test were to evaluate, depending on the considered flow rates, the occurrence of fluid recirculation, observed by tracking particle trajectories. Additionally, the study aimed to measure velocities in different zones of the biomodel. It's important to mention that the in-vitro study was conducted exclusively on the two biomodels produced using additive manufacturing molds.

For the case of the biomodel in which the inlet and outlet channels have an angle of 180° between them, six different flow rates were evaluated, i.e., 5 mL/min ($\Rightarrow$ Re (Reynolds Number)=1.95), 6.8 mL/min ($\Rightarrow$ Re=2.65), 10 mL/min ($\Rightarrow$ Re=3.90), 20 mL/min ($\Rightarrow$ Re=7.80), 50 mL/min ($\Rightarrow$ Re =19.49) and still 100 mL/min ($\Rightarrow$ Re=38.99).

In turn, for the case of the biomodel in which the inlet and outlet channels have an angle of 60° to each other, only the flow rates of 8 mL/min ($\Rightarrow$ Re=3.12), 15 mL/min ($\Rightarrow$ Re=5.85), 30 mL/min ($\Rightarrow$ Re=11.70) and 50 mL/min ($\Rightarrow$ Re=19.49) were inferred. It is noteworthy to refer that, for this second biomodel, the study started with a flow rate of 8 mL/min, because during the experimental test, this was the flow rate from which the phenomenon of recirculation began to be verified.

2.4 Evaluation of the Geometric Structure of the Molds and Biomodels

One of the requirements regarding the manufacture of biomodels is that their geometries must correspond to

the original STL (Standard Tessellation Language) model. In this sense, and with the aim of verifying this issue, images were acquired, both of the biomodels and of the aneurysms (molds) that originated the biomodels, using the inverted microscope used in the experimental tests. It should be emphasized that both the aneurysms and the biomodels measured were only those that showed a 50% reduction. Once the images were obtained, there were carried out measurements in the different locations, using the *ImageJ* software.

It's important to note that dimensions were evaluated for all three biomodels produced and studied in this work. This includes the two biomodels with polysmooth lost nuclei (featuring different geometries) and the biomodel with the glycerin-based soap core, although no experimental tests were conducted on the latter.

The dimensions of both the resin aneurysm and the polysmooth aneurysms with different geometries were assessed. It's worth highlighting that for the polysmooth aneurysms, measurements were taken both before and after the application of the superficial treatment.

To evaluate the geometric structure, measurements were taken at three specific locations. These measurements were conducted around the aneurysm and in each of its arms, as illustrated in Figure 2.

Figure 2: Schematic representation of the locations of the biomodel in which there were taken measurements to evaluate the geometric structure.

3 RESULTS

3.1 Results for the Evaluation of the Optical Transparency of the Biomodel

For the experimental work, a sheet with a rectangular structure was used in which each black or white rectangles had 2.4 x 3.9 mm of dimensions and under which the biomodel was placed. Thus, this structure aimed to allow the evaluation of the issue of optical distortion, caused by solid-liquid interaction.

Figure 3 presents the results for the biomodel using a polysmooth mold. Image (a) shows the

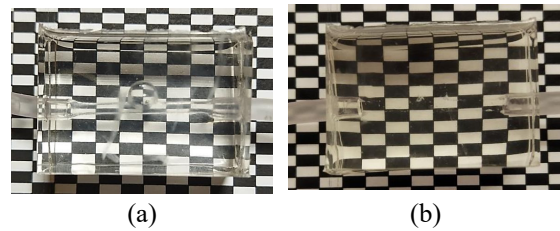biomodel when water was injected, while image (b) depicts the situation in with a glycerin-based solution.

Figure 3: Evaluation of the optical transparency of the biomodel. In this evaluation, the inlet and outlet channels have a 180° angle to each other, and a glycerin-based soap mold was used. Panel (a) represents the case with water as the fluid, while panel (b) shows the case with a glycerin-based solution.

Figure 4: Evaluation of the optical transparency of the biomodel, in which the inlet and outlet channels have an angle of 180° to each other, and where the mold used consisted of polysmooth, for the situation in which the fluid used was water (a) and for the case where the fluid was a glycerin-based solution (b).

To begin with, Figure 4 displays the results obtained for the biomodel using a glycerin-based soap mold. Image (a) corresponds to the biomodel with water injection, and image (b) depicts the situation with a glycerin-based solution.

One can see that, when water is used as the injected fluid (with a lower refractive index than PDMS), the mold walls are visible. In contrast, when a glycerin-based solution is used (with a matching refractive index to PDMS), the mold walls become invisible.

Additionally, it is worth noting that when water is used, there is some slight distortion and curvature of the rectangle structure, which is visible in all three biomodels. This effect is more pronounced in the case of the biomodel using a glycerin-based soap mold (as shown in Figure 3).

3.2 Qualitative Analysis of Flow Behaviour

The recorded images, using the Photron FASTCAM visualization software, were subsequently processed

using the *ImageJ* software. In particular, the particle trajectories were obtained using the *Z Project* plugin, and velocities using the *MTrackJ* plugin.

Firstly, the case of the biomodel in which the inlet and outlet channels have an angle of 180° between them. Thus, the trajectories of the PMMA particles, for a flow rate of 5 mL/min, 6.8 mL/min and 10 mL/min, resulting from the image processing, are shown in Figure 5.
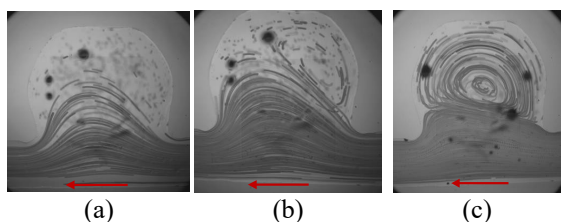

(a)   (b)   (c)

Figure 5: Trajectories of the PMMA particles, for a flow rate of 5 mL/min (Re=1.95), (a); 6.8 mL/min (Re=2.65), (b) and 10 mL/min (Re=3.90), (c). The arrow inserted in each image translates the direction of fluid circulation.

From observation of the previous figure, one can see that for a flow rate of 5 mL/min, (a), the phenomenon of fluid recirculation has not yet occurred.

In turn, for a flow rate of 6.8 mL/min, (b), the respective phenomenon is already beginning to be observed, although it is still reduced and only occurs in an area located inside the aneurysm. It should also be noted that this recirculation zone occurs on the fluid inlet side. On the other hand, for a flow rate of 10 mL/min, (c), it is visible that the recirculation phenomenon is already perfectly developed and covers almost the entire interior of the aneurysm.
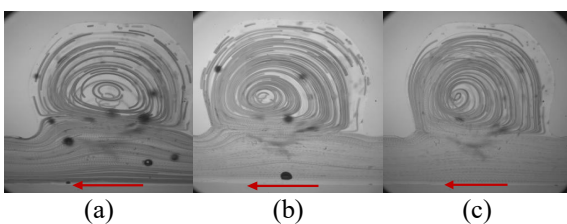

(a)   (b)   (c)

Figure 6: PMMA particle trajectories, for a flow rate of 20 mL/min (Re=7.80), (a4); 50 mL/min (Re=19.49), (a5) and 100 mL/min (Re=38.99), (a6). The arrow introduced in each image reflects the direction of fluid circulation.

After studying the trajectories of the PMMA particles for the three flow rates discussed previously, we now proceeded to study the flow rates of 20 mL/min, 50 mL/min and 100mL/min. Therefore, the particle trajectories for the aforementioned flow rates, and resulting from image processing, are shown in Figure 6.

By analyzing the previous figure, it is possible to observe that as the flow rate increases, the intensity of recirculation also increases. Additionally, it is noteworthy that the region of the aneurysm occupied by the recirculation phenomenon expands with the higher flow rates. For example, in the case of flow rates of 50 mL/min (b) and 100 mL/min (c), virtually all aneurysms exhibit recirculation. Furthermore, it is evident that with the increase in flow rate, the recirculation focus moves closer and closer to the aneurysm wall.

3.3 Results of the Geometric Assessment of Molds and Biomodels

Firstly, the dimensions of the mold which originated the final biomodel, in PDMS were evaluated. Two measurements were taken at each location and, subsequently, the average was calculated.

After obtaining the average values, these were then compared with the dimensions of the original STL model. This comparison was made by calculating the relative percentage error between both.

Therefore, in the following Table 2, there is a comparison made between the measurements obtained in *ImageJ* and the dimensions of the model in the STL file, for the resin mold.

Table 2: Comparison between the measurements obtained in ImageJ and the dimensions of the model in the STL file, by calculating the relative percentage error, for the resin mold.

Name	Length-*ImageJ* (mm)	Length-*Inventor* (mm)	Relative Error (%)
Aneurysm	4.934	5.00	1.33%
Left Arm	1.883	1.85	1.78%
Right Arm	1.809	1.85	2.22%

Analyzing the percentage errors obtained for the resin mold, it is possible to verify the existence of reduced errors in the order of 2%. The small value of these errors ends up proving, in a certain way, the good surface finish of the parts obtained by the MSLA (Masked Stereo Lithography Apparatus) additive manufacturing technique.

In a second phase, the dimensions of the final biomodel in PDMS was evaluated.

This means that there were also taken two dimensions at each location of the studied biomodel and, subsequently, these values were averaged. After

obtaining the average values, it was then compared with the dimensions of the original STL model. Once again, this comparison was made by calculating the relative percentage error between both.

Thus, Table 3 shows a comparison made between the measurements obtained in the *ImageJ* software and the dimensions of the model in the STL file, for the biomodel in which the lost nucleus was made of glycerin-based soap.

Table 3: Comparison between the measurements obtained in the *ImageJ* software and the dimensions of the STL file model, by calculating the percentage error, for the PDMS biomodel (in which the missing nucleus was made of glycerin-based soap).

Name	Length-*ImageJ* (mm)	Length-*Inventor* (mm)	Relative Error (%)
Aneurysm	5.204	5.00	4.07%
Left Arm	1.946	1.85	5.20%
Right Arm	1.885	1.85	1.86%

4 CONCLUSIONS

The main objective of this study was to investigate the flow in an idealized semi-rigid biomodel representing an intracranial aneurysm. The flow visualization tests identified areas within the aneurysm where fluid recirculation occurred. Notably, the central region of the aneurysm, where recirculation occurred, exhibited lower velocities compared to the inlet and outlet speeds. With an increase in the flow rate, the disparity between the velocity inside the aneurysm and the inlet and outlet velocities became more pronounced, indicating an expanded recirculation area within the aneurysm. Furthermore, an increase in the flow rate resulted in the recirculation focus moving closer to the aneurysm wall. It is highly recommended to conduct further studies concerning the aim of this paper, namely there should be performed numerical analysis for validating the experimental results for the two studied geometries. It is suggested to conduct numeric simulations in steady state and transient regime to infer if there are discrepancies between the velocity values determined experimentally and numerically. Apart from the validation of results, further numeric simulations will produce a more profitable use of the velocity and pressure profiles in terms of the prediction of aneurism geometries that are at high risk of rupture.

REFERENCES

Campo-Deaño, L.; Dullens, R.; Aarts, D.; Pinho, F.; Oliveira, M. (2013). Viscoelasticity of Blood and Viscoelastic Blood Analogues for Use in Polydymethylsiloxane in Vitro Models of the Circulatory System. *Biomicrofluidics*, *7*, 34102, doi:10.1063/1.4804649.

Ferguson G. G. (1972). Physical factors in the initiation, growth, and rupture of human intracranial saccular aneurysms. Journal of neurosurgery, 37(6), 666–677. https://doi.org/10.3171/jns.1972.37.6.0666.

Hopkins, L.M.; Kelly, J.T.; Wexler, A.S.; Prasad, A.K. (2000). Particle Image Velocimetry Measurements in Complex Geometries. *Exp. Fluids*, *29*, 91–95, doi:10.1007/s003480050430.

Inagawa T. (2010). Site of ruptured intracranial saccular aneurysms in patients in Izumo City, Japan. Cerebrovascular diseases (Basel, Switzerland), 30(1), 72–84. https://doi.org/10.1159/000314623.

Lasheras, J.C. (2006). The Biomechanics of Arterial Aneurysms. Annu. Rev. Fluid Mech., 39, 293–319, doi:10.1146/annurev.fluid.39.050905.110128.

Pinho, D.; Campo-Deaño, L.; Lima, R.; Pinho, F.T. (2017) In Vitro Particulate Analogue Fluids for Experimental Studies of Rheological and Hemorheological Behavior of Glucose-Rich RBC Suspensions. *Biomicrofluidics*, *11*, doi:10.1063/1.4998190.

Rodrigues, R.O.; Pinho, D.; Bento, D.; Lima, R.; Ribeiro, J. (2016). Wall Expansion Assessment of an Intracranial Aneurysm Model by a 3D Digital Image Correlation System. Measurement, 88, 262–270,

doi:https://doi.org/10.1016/j.measurement.2016.03.04 5.

Rodriguez-Régent, C.; Edjlali-Goujon, M.; Trystram, D.; Boulouis, G.; Ben Hassen, W.; Godon-Hardy, S.; Nataf, F.; Machet, A.; Legrand, L.; Ladoux, A.; et al. (2014) Non-Invasive Diagnosis of Intracranial Aneurysms. Diagn. Interv. Imaging, 95, 1163–1174, doi:https://doi.org/10.1016/j.diii.2014.10.005.

Roloff, C.; Bordás, R.; Nickl, R.; Mátrai, Z.; Szaszák, N.; Szilárd, S.; Thévenin, D. (2013). Investigation of the Velocity Field in a Full-Scale Model of a Cerebral Aneurysm. Int. J. Heat Fluid Flow, 43, 212–219, doi:https://doi.org/10.1016/j.ijheatfluidflow.2013.06.0 06.

Miranda, I.; Souza, A.; Sousa, P.; Ribeiro, J.; Castanheira, E.M.S.; Lima, R.; Minas, G. (2022). Properties and Applications of PDMS for Biomedical Engineering: A Review"*Journal of Functional Biomaterials* 13, 1: 2. doi: https://doi.org/10.3390/jfb13010002

Souza, A.; Souza, M.S.; Pinho, D.; Agujetas, R.; Ferrera, C.; Lima, R.; Puga, H.; Ribeiro, J. (2020) 3D Manufacturing of Intracranial Aneurysm Biomodels for Flow Visualizations: Low Cost Fabrication Processes. *Mech. Res. Commun.*, *107*, 103535, doi:10.1016/ j.mechrescom.2020.103535.

Souza, A. V. A. (2020b). Hemodynamic study in a real intracranial aneurysm: an in vitro and in silico approach," Dissertação de Mestrado, Instituto Politécnico de Bragança, Bragança/Portugal.

Steiger, H.J.; Liepsch, D.W.; Poll, A.; Reulen, H.J. (1988). Hemodynamic Stress in Terminal Saccular Aneurysms: A Laser-Doppler Study. *Heart Vessels*, *4*, 162–169, doi:10.1007/BF02058429.

Ye, J., Zheng, P., Hassan, M., Jiang, S., & Zheng, J. (2017). Relationship of the angle between the A1 and A2 segments of the anterior cerebral artery with formation and rupture of anterior communicating artery aneurysm. Journal of the neurological sciences, 375, 170–174. https://doi.org/10.1016/j.jns.2017.01.062